

MASS TRANSFER IN TIDALLY HEATED STARS ORBITING MASSIVE BLACK HOLES AND IMPLICATIONS FOR REPEATING NUCLEAR TRANSIENTS

PHILIPPE Z. YAO¹ AND ELIOT QUATAERT¹

¹Department of Astrophysical Sciences, Princeton University, Princeton, NJ 08544, USA
Version May 19, 2025

ABSTRACT

The structure of stars orbiting close to supermassive black holes (SMBHs) can be dramatically modified by tidal heating, which can in principle dissipate an energy much larger than the stellar binding energy. We use analytic models and MESA to explore the coupled dynamics of tidal heating, stellar structural evolution, orbital decay due to gravitational waves and tides, and mass transfer due to Roche lobe overflow. In contrast to more equal mass stellar binaries, the stable mass transfer rate for stars orbiting SMBHs is typically set by the tidal heating timescale (the timescale for tides to increase the stellar radius), not by the gravitational wave orbital decay timescale. The resulting stable mass transfer rate is sensitive to the tidal heating model but is plausibly $\sim 10^{-3} - 10^{-5} M_{\odot} \text{ yr}^{-1}$ (and perhaps larger), sufficient to produce low-luminosity active galactic nuclei in many galaxies. The stability of mass transfer is sensitive to *where* in the stellar interior the tidal energy is dissipated. MESA models confirm the expected result that mass transfer is unstable (stable) if tidal heating increases (decreases) the fraction of the star that is convective. More detailed conclusions about the stability of mass-transfer will require self-consistently calculating how the tidal heating of stars changes in response to internal structural changes produced by the tidal heating itself. Stars with tidal heating-induced mass transfer can produce a large population of low-luminosity active galactic nuclei; they may also be the progenitors of some partial tidal disruption candidates (e.g., ASASSN-14ko) as well as short period quasi-periodic eruptions (e.g., eRO-QPE2 and GSN 069). However, many repeating nuclear transients produced by tidal heating-induced mass loss are likely fainter than those detected thus far, and remain to be discovered.

Subject headings: binaries: general — quasars: supermassive black holes — stars: evolution — stars: mass-loss — transients: tidal disruption events

1. INTRODUCTION

The fate of stars orbiting close to supermassive black holes depends on the complex interplay of gravitational interactions and hydrodynamic processes such as tides, stellar collisions, and star-accretion disk collisions. For example, stars in a nuclear cluster can be scattered onto orbits where the pericenter passage intercepts the tidal radius, resulting in tidal disruption events (TDEs) (e.g. Hills 1975; Rees 1988). While TDEs have been systematically studied with over 100 candidates detected so far (e.g. Gezari 2021; Yao et al. 2023), their less extreme counterparts have become a recent focus of attention with the discovery of nearly a dozen repeating nuclear transients (RNTs) in the past few years by all-sky optical and X-ray surveys.

Multiple types of RNTs have been observed, including quasi-periodic eruptions (QPEs) and partial-tidal disruption candidates (pTDEs). QPEs are recurring soft X-ray flares with intervals ranging from hours to days, exhibiting diverse timing patterns and lacking bright optical or UV counterparts (e.g. Miniutti et al. 2019; Arcodia et al. 2021; Chakraborty et al. 2021, 2024, 2025; Arcodia et al. 2022; Miniutti et al. 2023a; Webbe & Young 2023; Arcodia et al. 2024). In contrast, pTDEs such as ASASSN-14ko (Payne et al. 2021), eRASS1 J045650.3-203750 (Liu et al. 2023a), and AT2022dbl (Hinkle et al. 2024; Makrygianni et al. submitted) produce flares in optical, UV, and/or X-ray with a significantly longer mean recurrence time. For ASASSN-14ko, with a mean period of 114.2 ± 0.4 days and flare duration of ~ 10 days, a period derivative is also observed at $\dot{P} \approx -0.0026 \approx -(7\text{h})/P_0$

(Payne et al. 2022), significantly more rapid orbital evolution than can be produced by gravitational wave inspiral of a star (Payne et al. 2021).

Observations of RNTs are suggestive of their origin in a binary system consisting of a solar mass object orbiting a supermassive black hole (SMBH) (see, e.g., Xian et al. 2021; Suková et al. 2021; Krolik & Linial 2022; Linial & Metzger 2023, 2024; Lu & Quataert 2023; Franchini et al. 2023; Liu et al. 2023b, 2025; Linial & Quataert 2024b; Bandopadhyay et al. 2024; Yao et al. 2025). What distinguishes them from each other in such models is orbital parameters and black hole mass. For QPEs, the alternating long-short time between flares in GSN 069 and eRO-QPE2 (Miniutti et al. 2019, 2023a; Arcodia et al. 2021) suggests a star on a mildly eccentric orbit with a period of hours to days. Host galaxy studies also indicate that the black hole masses are $\sim 10^5 - 10^6 M_{\odot}$ (e.g. Wevers et al. 2022). In contrast, pTDEs may arise from stars on highly eccentric orbits with periods of months to years (Payne et al. 2021; Cufari et al. 2022; Liu et al. 2023b; Bandopadhyay et al. 2024; Liu et al. 2025).

Even if the pericenter distance of the star is outside its tidal radius, the orbiting star can be strongly affected by the tidal force of the SMBH via dissipation of tidal energy. Previous work has shown that interior to a pericenter distance of $\sim 4-5r_t$ (where $r_t = R_{\star}(M_{\bullet}/M_{\star})^{1/3}$ is the tidal disruption radius), this can lead to runaway expansion of the stellar radius, initiating mass transfer onto the central black hole (Li & Loeb 2013; Lu et al. 2021; Linial & Quataert 2024a,b). Indeed, it is likely inevitable that tidal heating changes the structure of most stars approaching a SMBH secularly, e.g., by gravitational

*E-mail: philippe.yao@princeton.edu

wave orbital decay or by small scattering-induced changes in pericenter distance for stars on highly eccentric orbits – the empty loss cone regime of stellar dynamics in galactic nuclei.

In this paper, we build on previous work on tidally heated stars near SMBHs to study the fate of these stars both analytically and in 1D MESA simulations. We focus for concreteness on Sun-like stars on either mildly or highly eccentric orbits around SMBHs. As in more equal mass binaries, there are likely regimes of both stable and unstable mass transfer (e.g. Paczyński 1971; Hjellming & Webbink 1987; Ge et al. 2015). An important difference between the high mass ratio case relevant to stars around SMBHs and the more equal mass case of stellar binaries is that the high mass ratio makes it more likely that mass transfer is unstable (Linial & Sari 2023; Lu & Quataert 2023). This is because it is difficult for the angular momentum lost from the star via mass transfer to return to the orbit, for three separate reasons: (1) tidal torques between the star and the disk are inefficient at high mass ratio (analogous to the inability of Earth-mass objects to open gaps in protostellar disks), (2) mass transfer via L2 is efficient at high mass ratio and extracts angular momentum from the orbit (Linial & Sari 2017), (3) the proximity of the tidal radius to the last stable circular orbit implies that a significant amount of angular momentum can be accreted by the black hole. Taken together these results suggest that the star’s orbit may not evolve significantly in response to mass loss. In this case, the stability of mass transfer is largely set by the star’s response to mass-loss: if $R_\star \propto M_\star^\zeta$ with $\zeta \lesssim 1/3$, the mass transfer will likely be unstable. This suggests that mass-transfer by fully convective stars will be unstable, while that by radiative stars will be stable (Lu & Quataert 2023). The two regimes of mass transfer for stars orbiting SMBHs will have very different observational outcomes. For example, stable mass transfer may power long-lived low-luminosity active galactic nuclei (Hameury et al. 1994; MacLeod et al. 2013). On the other hand, unstable mass transfer would produce a runaway process that leads to super-Eddington accretion, appearing as a transient flare akin in some ways to TDEs (Linial & Quataert 2024b).

The primary goal of this paper is to identify qualitatively new features of mass-transfer in tidally heated stars and assess their possible observational implications. Solving the full coupled problem of orbital and stellar evolution for stars near a BH’s tidal radius is formidable, so it is worth stressing up front a few of the assumptions and limitations of our analysis. These simplifying assumptions are made largely because of uncertainties in the key tidal heating physics. The first is that we will use models of tidal heating that depend only on the global properties of the star (mass, radius) and its pre-tidal-heating stellar structure. This is in general not a good assumption because tidal heating changes the stellar structure significantly (as we shall show), which would in turn change the tidal excitation of waves and the resulting tidal heating rate. Secondly, we will not attempt to calculate in detail where in the star the tidal energy is dissipated, despite this being important for determining how the star responds to tidal heating. Instead, we will use phenomenological models for how tidal energy is spatially distributed. And, finally, our analysis will include both mildly eccentric and highly eccentric orbits. The reader should be warned up front that our theoretical tools (analytics and MESA) are better suited to lower eccentricity orbits, but we believe they also provide qualitative insight into the role of tidal heating for stars on highly eccentric orbits. We return to prospects for relaxing these assumptions in §4.

The remainder of this paper is organized as follows. We outline our analytic model and show the resulting orbital and stellar evolution for a Sun-like star in §2. We then carry out similar calculations conducted with more realistic stellar models with MESA in §3. Our simulations cover a wide range of orbital parameters and tidal heating models, and are evolved until unstable mass transfer commences. We explore the implications of the stable and unstable mass transfer phases seen in our calculations for recently discovered RNTs and provide a discussion and summary of our models and findings in §4.

2. STABLE MASS TRANSFER WITH TIDAL HEATING

Consider a star of mass M_\star in orbit around a supermassive black hole of mass $M_\bullet \gg M_\star$. The orbital period is P , the star’s eccentricity is e and the pericenter distance r_p is comparable to the tidal radius $r_t \simeq R_\star (M_\bullet/M_\star)^{1/3}$. Gravitational wave radiation causes significant orbital decay on a timescale τ_{GW} , eventually leading to mass transfer when $r_p = 2r_t$. Considering first a case without tidal heating, the stable mass transfer rate would be set by angular momentum loss driven by gravitational wave radiation. For highly eccentric ($1 - e \ll 1$) and near-circular ($e \ll 1$) orbits, this timescale can be approximated as:

$$\begin{aligned} \tau_{\text{GW,para}} &\sim \frac{r_p}{|\dot{r}_p|} = \frac{24\sqrt{2}}{59} \frac{c^5}{G^3} \frac{r_p^{5/2} a^{3/2}}{M_\bullet^2 M_\star} \\ \tau_{\text{GW,circ}} &\sim \frac{a}{|\dot{a}|} = \frac{5}{64} \frac{c^5}{G^3} \frac{a^4}{M_\bullet^2 M_\star} \end{aligned} \quad (1)$$

The resulting stable mass transfer solution has a mass transfer rate from the star to the BH of $\dot{M} \sim M_\star/\tau_{\text{GW}}$

$$\begin{aligned} \dot{M}_{\text{GW,para}} &\simeq 4.6 \times 10^{-10} M_\odot \text{yr}^{-1} \left(\frac{R_\star}{R_\odot} \right)^{-5/2} \\ &\quad \left(\frac{M_\star}{M_\odot} \right)^{17/6} \left(\frac{M_\bullet}{10^6 M_\odot} \right)^{2/3} \left(\frac{P}{100 \text{days}} \right)^{-1} \\ \dot{M}_{\text{GW,circ}} &\simeq 10^{-6} M_\odot \text{yr}^{-1} \left(\frac{R_\star}{R_\odot} \right)^{-4} \left(\frac{M_\star}{M_\odot} \right)^{10/3} \left(\frac{M_\bullet}{10^6 M_\odot} \right)^{2/3} \end{aligned} \quad (2)$$

The above calculation neglects the fact that tides raised in the star by the BH can deposit sufficient energy to dramatically change the structure of the star before mass transfer is initiated at $r_p = 2r_t$. Heat deposited inside the star will increase its radius when the integrated tidal energy deposited is a fraction of the stellar binding energy (as we shall see, the heating timescale near r_t is less than the thermal time of the low mass stars we focus on in this paper so the tidal energy cannot be efficiently radiated away). Because the orbital energy of a star near r_t is a factor of $\sim (M_{\text{BH}}/M_\star)^{2/3}$ larger than its binding energy, tidal energy dissipation of just a small fraction of the orbital energy can unbind the star. Linial & Quataert (2024b) showed that standard estimates of tidal heating predict that the tidal energy dissipated on the gravitational wave inspiral time is indeed large enough to unbind the star (see also Li & Loeb 2013; Lu et al. 2021 for related calculations). These results imply that tidal heating will inflate the radius of the star, leading to mass transfer earlier than would be expected absent tidal heating. For now, we assume that the resulting mass transfer is stable (although this is by no means guaranteed), and quantify the properties of this unusual regime of stable

mass transfer. In the presence of strong tidal heating, the stable mass transfer solution is no longer set by τ_{GW} , but is instead set by the tidal heating timescale $\tau_{\text{heat}} \sim E_{\star}/\dot{E}_{\text{tides}}$ when $\tau_{\text{heat}} < \tau_{\text{GW}}$. We show later in this section that this is often the case.

2.1. Effects of Tidal Heating

In what follows, we consider stars on both roughly circular ($e \ll 1$) and highly eccentric ($1 - e \ll 1$) orbits (the results for tidal heating are cleanest in these two regimes). For stars on highly eccentric orbits, the black hole's tidal potential excites significant internal stellar oscillation modes at each pericenter passage. The amount of heating in this regime can be estimated via the linear perturbation theory of [Press & Teukolsky \(1977\)](#). We assume that non-linear coupling between modes excites an abundance of daughter modes after pericenter passage, which quickly dissipates the tidally excited modes ([Kumar & Goodman 1996](#); [Linial & Quataert 2024a](#)). When this is the case and the damping time of the tidally excited oscillations is much shorter than the orbital period, the time-averaged tidal heating rate can be approximated as

$$\dot{E}_{\text{tides,p}} \simeq \frac{GM_{\star}^2/R_{\star}}{P} f(\chi) \quad (3)$$

where $\chi \equiv r_p/r_t$. For a Sun-like star on a highly eccentric orbit near mass transfer ($\chi \sim 2$), we take $f(\chi) \simeq 0.33 f_p \chi^{-\alpha}$ with $\alpha \simeq 15$ based on the calculations in [Lai \(1997\)](#) which generalize those of [Press & Teukolsky \(1977\)](#) and [Lee & Ostriker \(1986\)](#) to a rotating star. In this expression for $f(\chi)$, f_p is a dimensionless number intended to encapsulate the uncertainty in the tidal heating theory for highly eccentric orbits. The expression here for the energy transfer assumes that the star has been spun up to the point where its rotation rate no longer evolves significantly due to tides. This is a reasonable assumption because the tidal spin-up time is shorter than other key timescales in the problem (e.g., the GW inspiral time, the tidal heating time, etc.). A useful numerical calibration of the linear theory results leading to equation 3 is provided by the simulations of [Cufari et al. \(2023\)](#), who simulated the tidal energy deposited in an $n = 3/2$ polytrope and found $\Delta E \simeq 0.02 GM_{\star}^2/R_{\star}$ for $r_p \simeq 2r_t$. This is only a factor of few higher than the linear tidal calculations of [Lee & Ostriker \(1986\)](#). [Cufari et al. \(2023\)](#)'s tidal heating rate is significantly larger than our default $f(\chi)$ from [Lai \(1997\)](#) in part because solar-type stars are better approximated by $n = 3$ polytropes and in part because the tidal energy deposition decreases significantly when the star is rapidly rotating ([Lai 1997](#); [Kumar & Quataert 1998](#)).

When the non-linear dissipation time of the tidally excited modes is longer than the orbital period, the resulting tidal energy input rate and heating rate are not given by eq 3. Instead, the tidally excited modes can be chaotically driven to even larger amplitudes, leading to larger heating rates than assumed here (e.g. [Mardling 1995a,b](#); [Wu 2018](#); [Vick & Lai 2018](#)).

For a solar-type star with a radiative core and a convective envelope, dynamical tidal dissipation through internal gravity waves can also produce significant heating inside the star ([Goodman & Dickson 1998](#)). In the case of a low-eccentricity and short-period orbit of a solar-mass star around a massive BH, the tidal heating rate can be estimated via ([Linial](#)

& Quataert 2024b)

$$\dot{E}_{\text{tides,c}} \simeq 4 \times 10^{38} \text{ erg s}^{-1} f_c e^2 \left(\frac{a}{2r_t} \right)^{-23/2}, \quad (4)$$

where f_c is a dimensionless number intended to capture the uncertainty in the tidal heating theory for circular orbits. In particular, inertial wave excitation in convection zones can potentially lead to $f_c \gg 1$ ([Barker 2020](#)), so we will consider that possibility as well in some of our calculations ([Linial & Quataert 2024b](#) estimated $f_c \sim 100$ for inertial wave excitation in solar-type stars). Note that equation 4 should in general include a dependence on the stellar mass and the internal structure of the star (e.g., its evolutionary state or its tidally-modified structure). We neglect this dependence for this initial exploration, but return to this point in §4.

For the analytic estimates in this section, we neglect radiative losses, motivated by the fact that the tidal heating timescale near r_t is typically shorter than the thermal time of low mass stars (this assumption will be relaxed in our MESA models in §3). In this case, we can calculate the evolution of the star's properties via

$$\frac{dE_{\text{tot}}}{dt} = -\phi_E \frac{d}{dt} \frac{GM_{\star}^2}{R_{\star}} = \dot{E}_{\text{tides}} \quad (5)$$

where E_{tot} is the total energy of the star, and ϕ_E depends on the structure of the star. For a Sun-like star, $\phi_E \simeq 0.82$.

When the total tidal heating becomes a fraction of the stellar binding energy, the stellar structure will gradually be modified, reflected primarily by an expansion in radius. Prior to the onset of RLO and mass loss, the radius of the star will increase in response to significant tidal heating, implying that mass loss via RLO then becomes inevitable. Once RLO commences and the star transfers mass to the BH, equation 5 becomes

$$\phi_E \left(\frac{d \ln R_{\star}}{dt} - 2 \frac{d \ln M_{\star}}{dt} \right) = \frac{\dot{E}_{\text{tides}}}{E_{\star}}, \quad (6)$$

where $E_{\star} \equiv GM_{\star}^2/R_{\star}$ is of order the binding energy of the star. We now assume, following [Lu & Quataert \(2023\)](#) and [Linial & Sari \(2023\)](#), that once mass transfer commences, the angular momentum and energy lost from the star via mass loss is permanently lost and cannot be returned to the orbit (as discussed in the introduction, the authors of these studies argue that this is appropriate for the high mass ratio limit of a star around a massive BH). This implies that the orbit does not change in response to mass loss. Since r_p is fixed, maintaining $r_p \simeq 2r_t$ as M_{\star} and R_{\star} change requires $R_{\star} \propto M_{\star}^{1/3}$. This is the stable mass transfer solution, specialized to the case of constant r_p ; stable mass transfer further assumes that the stellar radius does not intrinsically expand more rapidly than $R_{\star} \propto M_{\star}^{1/3}$ in response to mass loss (we study this in MESA in §3). If we substitute $R_{\star} \propto M_{\star}^{1/3}$ into equation 6 and use $r_p = 2r_t$, we can solve a simple ODE to obtain the mass transfer rates for the two types of orbits

$$\begin{aligned} \dot{M}_{\star,\text{para}}(t) &= -C_0 M_{\star,\text{MT}} \exp(-C_0 t) \\ \dot{M}_{\star,\text{circ}}(t) &= -C_1 \left(M_{\star,\text{MT}}^{5/3} - \frac{5}{3} C_1 t \right)^{-2/5}, \end{aligned} \quad (7)$$

where

$$C_0 = \frac{1}{5} \frac{f_p \chi_{\text{MT}}^{-15}}{P \phi_E}; \quad C_1 = \frac{3}{5} \frac{L_0 f_c}{\phi_E G} \frac{R_{\star,\text{MT}}}{M_{\star,\text{MT}}^{1/3}} e^2 (1-e)^{23/2}, \quad (8)$$

$L_0 = 4 \times 10^{38} \text{ erg s}^{-1}$ (Eq. 4), MT refers to stellar or orbital properties at the onset of mass transfer, and t measures time since the onset of RLO. Evaluated at this time, the mass transfer rate is

$$\begin{aligned} \dot{M}_{\star, \text{para}}(t_{\text{MT}}) &= 7.5 \times 10^{-5} M_{\odot} \text{yr}^{-1} \frac{M_{\star, \text{MT}}}{M_{\odot}} \left(\frac{P_{\text{MT}}}{100 \text{ days}} \right)^{-1} f_p \\ \dot{M}_{\star, \text{circ}}(t_{\text{MT}}) &= 2.4 \times 10^{-3} M_{\odot} \text{yr}^{-1} \frac{R_{\star, \text{MT}}}{R_{\odot}} \left(\frac{M_{\star, \text{MT}}}{M_{\odot}} \right)^{-1} \\ &\quad f_c e_{\text{MT}}^2 (1 - e_{\text{MT}})^{23/2}. \end{aligned} \quad (9)$$

When scaled to properties of typical solar-mass stars, the stable mass transfer rate estimated including tidal heating (Eq. 7) is significantly larger than simple estimates based on gravitational wave orbital decay (Eq. 2). This strongly suggests that the properties of stable mass transfer for stars orbiting massive black holes are set by mass loss initiated by tidal inflation of the stellar radius rather than by gravitational wave-induced orbital decay. This conclusion is subject to the non-negligible uncertainty in the tidal heating rate, but the large difference in the normalization of eq. 7 relative to eq. 2 suggests that it is robust (recall again that $f_p \gtrsim 1$ and $f_c \gtrsim 1$ are quite plausible). A corollary of this conclusion is that the stable mass transfer phase is likely to last at most of order $10^3 - 10^4$ yrs (and possibly less) instead of $10^6 - 10^7$ yrs based on gravitational wave orbital decay.

Tidal heating transfers energy from the orbit to the star, which can in turn modify the orbital properties. For highly eccentric orbits, the dominant effect is the change in orbital period, whereas for near-circular orbits it is the change in eccentricity. Their timescales at the onset of mass transfer are

$$\begin{aligned} \left(\frac{P}{\dot{P}} \right)_{\text{tides, para}} &\simeq \frac{10^6 \text{ yrs}}{f_p} \frac{R_{\star, \text{MT}}}{R_{\odot}} \left(\frac{M_{\star, \text{MT}}}{M_{\odot}} \right)^{-1} \\ &\quad \left(\frac{M_{\bullet}}{10^6 M_{\odot}} \right)^{2/3} \left(\frac{P_{\text{MT}}}{100 \text{ days}} \right)^{1/3} \\ t_{\text{tides, circ}} &\sim \frac{e}{\dot{e}} \simeq \frac{1.9 \times 10^5 \text{ yrs}}{f_c} \left(\frac{M_{\star, \text{MT}}}{M_{\odot}} \right)^{4/3} \\ &\quad \left(\frac{M_{\bullet}}{10^6 M_{\odot}} \right)^{2/3} \left(\frac{R_{\star, \text{MT}}}{R_{\odot}} \right)^{-1}. \end{aligned} \quad (10)$$

Equation 10 shows that the effect of orbital evolution by tides takes place 2-3 orders of magnitude slower than the corresponding mass transfer timescales evaluated from Equation 9. Thus, once mass transfer commences, orbital evolution by both tides and gravitational waves is generally slower. For our fiducial parameters ($f_p = f_c = 1$), gravitational wave orbital decay dominates over tides for the orbital evolution prior to the onset of mass transfer, but tidally-induced orbital changes will likely be more important if $f_p \gg 1$ or $f_c \gg 1$.

2.2. Mass, Radius, and Orbital Evolution with Gravitational Waves and Tidal Heating

Here we combine tidal heating and gravitational wave orbital decay for a solar-mass main sequence star to develop a simple model for the orbital and stellar evolution from the onset of stellar expansion due to tidal heating, to RLO and the onset of mass transfer from the star to the BH, to the end of the stable mass transfer phase. The calculations here *assume* stable mass transfer and do not follow the internal stellar

structure, and so cannot directly assess the validity of this assumption. We return to this point in §3. Orbital evolution here is given by gravitational waves (Peters 1964) as well as tides (although tides are subdominant for our fiducial parameters per eq. 10). For the latter we consider tidal circularization for nearly-circular orbits but include both \dot{E}_{tides} and \dot{J}_{tides} for the highly eccentric case, with $\dot{J}_{\text{tides}} \simeq \dot{E}_{\text{tides}}/2\Omega_p$.

As in §2.1, we assume mass transfer is initiated and maintained at $r_p \simeq 2r_t$, such that $R_{\star} = \frac{a(1-e)}{2M_{\bullet}^{1/3}} M_{\star}^{1/3}$; in this case, we can numerically solve for the evolution of the stellar radius using

$$\begin{aligned} (\dot{M} = 0) \quad \frac{d \ln R_{\star}(t)}{dt} &= \frac{\dot{E}_{\text{tides}}}{E_{\star} \phi_E} \\ (\dot{M} > 0) \quad \frac{d \ln R_{\star}(t)}{dt} &= \frac{6}{5} \frac{\dot{a}}{a} - \frac{6}{5} \frac{\dot{e}}{1-e} - \frac{\dot{E}_{\text{tides}}}{5 E_{\star} \phi_E}, \end{aligned} \quad (11)$$

where \dot{E}_{tides} , \dot{a} , and \dot{e} are functions of the evolving orbital and stellar parameters.

Figures 1 & 2 show the solutions to Equation 11 before (*left*) and after (*right*) the onset of mass transfer at $r_p = 2r_t$ for highly eccentric and near-circular orbits, respectively. Runaway expansion of the stellar radius before mass transfer is evident in both cases since the tidal heating rate is a strong function of the stellar radius. For both cases, we note that the tidal orbital evolution timescale (τ_{tides}) always remains subdominant when compared to τ_{GW} , which is itself small compared to τ_{heat} when mass transfer begins. Hence, orbital evolution by tides is not very important for these fiducial parameters.

2.2.1. Highly Eccentric Orbits

For the solar-type stars on highly eccentric orbits in Figure 1, we assume an initial orbit period of 114.2-day around a $7 \times 10^7 M_{\odot}$ SMBH, inspired by estimated parameters of ASASSN-14ko (Payne et al. 2021). The basic evolutionary results are not sensitive to reasonable changes to these assumed parameters. We initialize the orbit starting at a range of tidal heating parameters ($\chi \equiv r_p/r_t$), which also corresponds to a range of initial eccentricities.

As expected, stars with lower χ_i , i.e., smaller initial pericenter radii, quickly inflate due to tidal heating and rapidly reach $\chi = 2$, when mass transfer begins. For stars with larger initial pericenter distances (larger χ_i), the tidal heating is initially smaller; the longer initial tidal heating timescale means that there is more significant orbital decay of the semi-major axis due to gravitational wave emission prior to the onset of mass transfer. In all cases, after $\sim 10^4 - 10^7$ yrs, the stable mass transfer phase commences. The timescale for the onset of mass-transfer in the left panels of Figure 1 is largely set by the time it takes tidal energy deposition to increase the stellar radius by order unity given the initial value of χ_i (gravitational wave and tidal changes to the pericenter distance operate on yet longer timescales). The models here thus implicitly require the star to be placed on a long-period orbit with $\chi_i \sim 2 - 5$ by a mechanism such as the Hills mechanism (e.g. Hills 1988; Cufari et al. 2022; Lu & Quataert 2023; Linial & Sari 2023).

As we derived in equations 7 & 9, the mass transfer rate \dot{M}_{\star} decays exponentially and depends only on the initial orbital period at mass transfer. Also consistent with the analytics, the tidal heating timescale $\tau_{\text{heat}} \sim E_{\star}/\dot{E}_{\text{tides}}$ remains much shorter than the gravitational wave timescale and determines the stable mass transfer rate.

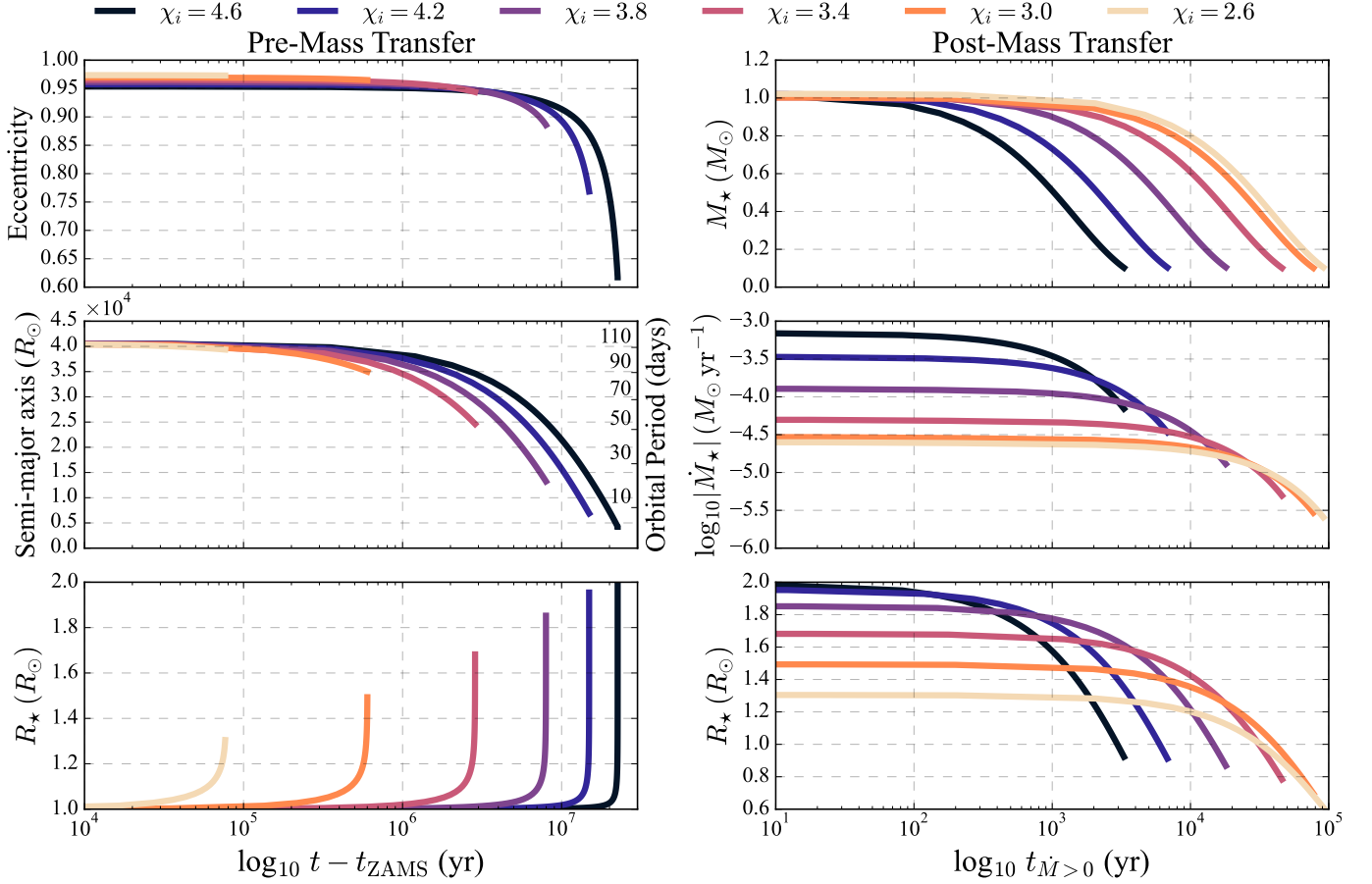


FIG. 1.— *Highly Eccentric Orbits*: Toy numerical solution for the evolution of orbital and stellar properties (eq. 11) for stars orbiting a $7 \times 10^7 M_\odot$ SMBH before (left) and after (right) the onset of mass transfer at $r_p = a(1 - e) = 2r_t$. The models shown are for a $1R_\odot$ & $1M_\odot$ star at t_{ZAMS} , have an initial orbital period $P_i = 114.2$ days, and a range of initial tidal heating parameters $\chi_i \equiv r_p/r_t$, which is equivalent to a range of initial eccentricities. Prior to RLO the orbit decays due to GWs and the stellar radius increases due to tidal heating. The mass transfer rate after RLO is set by the tidal heating timescale, and is significantly higher than predicted by gravitational wave orbital decay.

2.2.2. Near-circular Orbits

For solar-type stars on mildly eccentric orbits in Figure 2, we adopt a lower mass for the SMBH ($M_\bullet = 3 \times 10^6 M_\odot$), inspired by the estimated parameters of QPE hosts (Wevers et al. 2022). We test four cases, each representing a combination of initial eccentricity (0.3 or 0.5) and orbital period (4 or 7 days), which all allow the system to evolve to $r_p = 2r_t$ before their main sequence lifetime concludes. All models are subject to tidal heating following Equation 4, start with a high χ_i (and hence low $E_{\text{heat,c}}$), and undergo significant orbital decay to more mild eccentricities due to gravitational wave circularization. The final semi-major axis at mass transfer (a_{MT}) corresponds to orbital periods of 0.4 - 0.8 days.

Similar to the high-eccentricity case, stars on orbits with the smallest a_i inflate the fastest due to tidal heating and reach $\chi = 2$. Models with a greater a_i require a longer heating time, undergo more appreciable orbital decay, and end up mass transferring at lower eccentricities. This is because, unlike the highly eccentric calculations in Figure 1, gravitational waves circularize the mildly eccentric orbits much more rapidly within $\sim 10^7 - 10^8$ yrs, until tidal heating takes over to dominate the subsequent evolution. The mass transfer rate $\dot{M}_\star \sim 10^{-6} - 10^{-4} M_\odot/\text{yr}$ is set again by the tidal heating timescale, although for most of the evolution it is only a factor of $\sim 10 - 100$ times larger than the mass-transfer rate from

GWs alone (this is because e^2 is small at the onset of mass transfer, making eq. 9 more similar to eq. 2). We terminate the calculation when M_\star falls below $0.1 M_\odot$, where many models have already started to exhibit a diverging mass transfer rate expected from eq. 7.

We also show a case with a significantly higher tidal heating rate ($f_c = 100$) in Figure 3 with the same set of initial parameters as in Figure 2. As argued in the discussion below eq. 4, this level of heating is plausible. Here, the runaway expansion of the stellar radii is even more rapid, which leads to an earlier onset of mass transfer, less significant orbital evolution, and greater $R_{\star,\text{MT}}$ compared to the $f_c = 1$ case in Figure 2. The final semi-major axis at mass transfer (a_{MT}) corresponds to orbital periods of 1.6 - 2.3 days. Despite a significantly shorter tidal circularization timescale, the orbital evolution is still largely dominated by gravitational-wave orbit decay. By the onset of mass transfer, however, tidal heating again dominates the evolution, setting the much higher stable mass transfer rate of $\dot{M}_\star \sim 10^{-4} - 10^{-2} M_\odot/\text{yr}$ (as expected given $\dot{M}_\star \propto f_c$ in eq. 9).

3. NUMERICAL MODELS WITH MESA

The analytic model presented in §2 provides simple scaling relationships for the stable mass transfer rate as a function of stellar and orbital parameters, and the tidal heating model. However, it does not capture the stability of mass transfer or

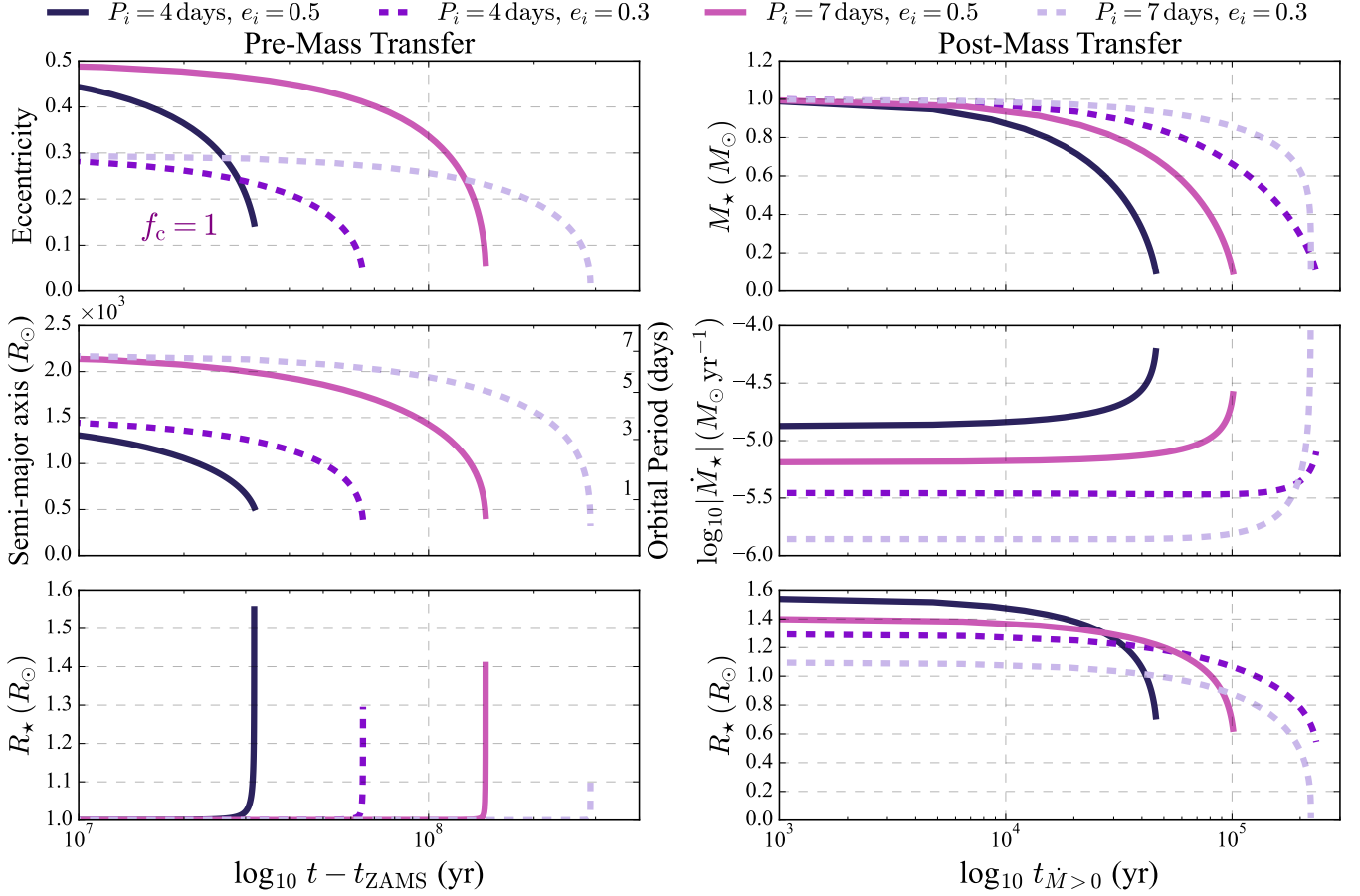


FIG. 2.— *Near-circular Orbits* ($f_c = 1$): Toy numerical solution for the evolution of orbital and stellar properties (eq. 11) for stars orbiting a $3 \times 10^6 M_\odot$ SMBH before (left) and after (right) the onset of mass transfer at $r_p = a(1 - e) = 2r_t$. The models shown are for a $1R_\odot$ & $1M_\odot$ star at t_{ZAMS} and have an initial eccentricity $e_i = 0.3$ (dashed lines) or $e_i = 0.5$ (solid lines) and an initial orbital period P_i of 4 or 7 days. As in Figure 1, the mass transfer rate is again largely set by the tidal heating timescale, but for the most circular orbits this is only a few times higher than $\dot{M}_{\text{GW,circ}}$ derived in eq. 2.

how tidal heating changes the internal structure of the star. Here, we perform more detailed calculations of tidally heated stars orbiting SMBHs with the Module for Experiments in Stellar Astrophysics (MESA, Paxton et al. 2011, 2013, 2015, 2018, 2019). All our binary MESA models consist of a point mass SMBH orbited by a $1 M_\odot$ zero-age main sequence (ZAMS) star.

Following the arguments summarized in the introduction, in our MESA simulations we assume that the angular momentum and energy lost from the star during mass-transfer are not returned to the orbit. By default, MESA does not handle gravitational wave orbital decay for eccentric orbits (circular options are included in MESA). Hence, we add dL/dt and de/dt terms¹ following Peters (1964) in all our orbit evolution with additional terms described in §2.2 to include effects of tidal orbital evolution (the latter are negligible for the calculations presented here). Furthermore, for tidal heating, we deposit energy in the star based on its evolving stellar and orbital properties. The spatial distribution of tidal heating in stellar interiors is uncertain and depends on the detailed mechanism of tidal dissipation. Such dissipation is plausibly non-linear for the large tidal distortions considered here. We will consider two possibilities in our MESA models that bracket the stellar response to tidal heating in a manner described below,

both with uniform heating per unit mass²:

1. Centrally Concentrated: $0.1 < r/R_\star < 0.2$. This is motivated by non-linear wave breaking of internal gravity waves due to geometric focusing in stellar cores (Goodman & Dickson 1998). Centrally concentrated heating also drives convection, promoting unstable mass transfer.
2. Uniform (per unit mass) throughout the Star: $0.25 < r/R_\star$. While this is less directly physically motivated, applying constant heating per unit mass raises the entropy more in the cooler outer regions, which inhibits convection and thereby stabilizes mass transfer.

As in Section 2, we use Equations 3 & 4 to calculate the heating power associated with stars in highly eccentric orbits and mildly eccentric orbits, respectively. We note that this time-averaged approximation is more accurate for persistent heating in the latter case, while highly eccentric orbits should receive heating predominantly near each pericenter passage in short bursts with the large-amplitude tidally excited waves damped by non-linear processes (Kumar & Goodman 1996).

For our MESA models, we consider the mass transfer stable or unstable when the stellar radius decreases or increases in

¹ In MESA, this corresponds to `jdot_extra_routine` and `edot_extra_routine` in `run_binary_extras`

² We avoid heating the stellar core at the smallest radii to prevent creating an artificial steep temperature gradient, which we found can lead to small numerical timesteps.

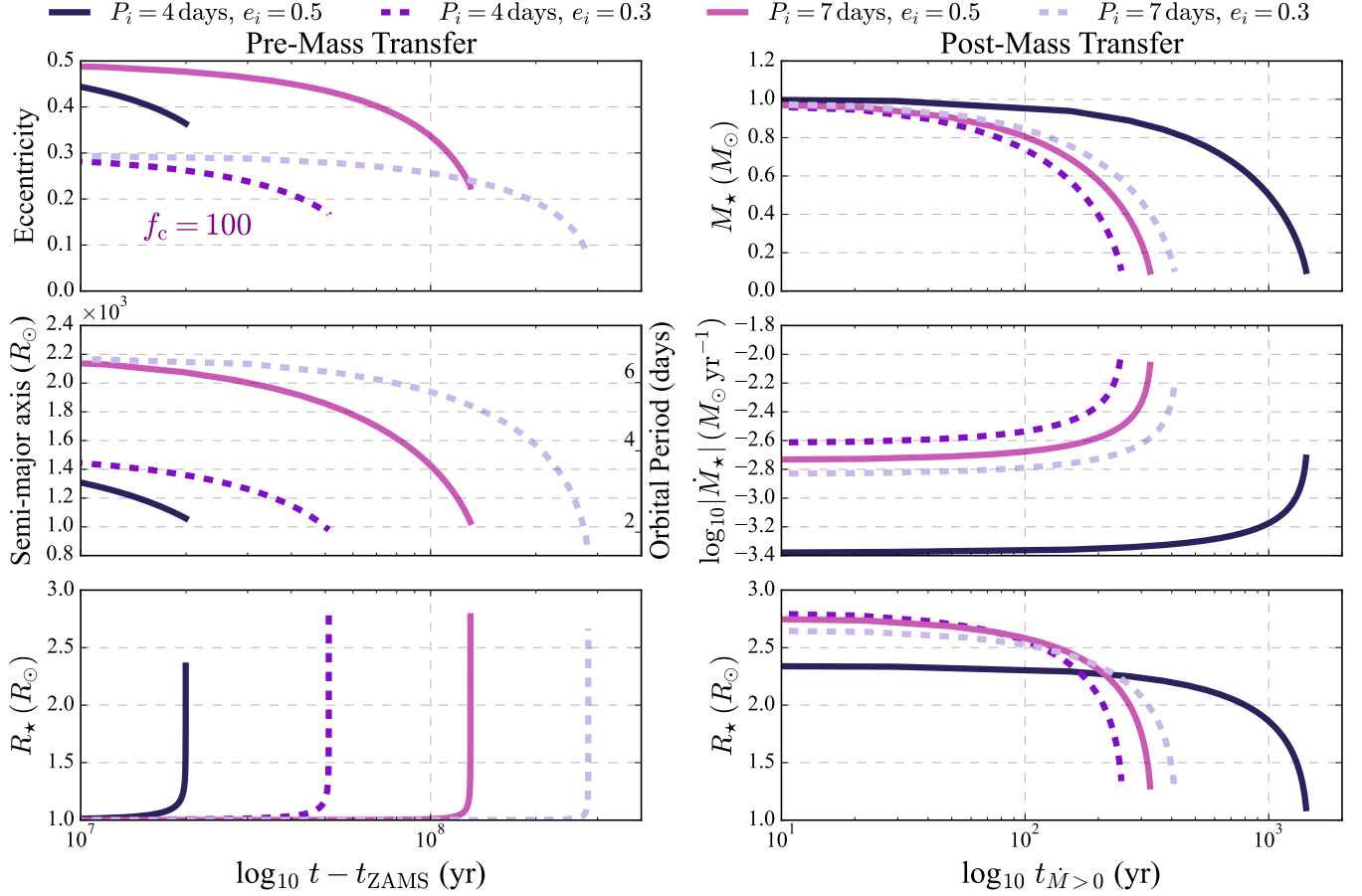


FIG. 3.— *Near-circular Orbits* ($f_c = 100$): Toy numerical solution for the evolution of orbital and stellar properties (eq. 11) for stars orbiting a $3 \times 10^6 M_\odot$ SMBH before (left) and after (right) the onset of mass transfer at $r_p = a(1 - e) = 2r_t$. The tidal heating is our fiducial model (eq. 4) multiplied by $f_c = 100$ to explore the impact of larger tidal heating rates. The models shown are for a $1 R_\odot$ & $1 M_\odot$ star at t_{ZAMS} with an initial eccentricity $e_i = 0.3$ (dashed lines) or $e_i = 0.5$ (solid lines) and an initial orbital period P_i of 4 or 7 days. For the larger tidal heating rate considered here, the star inflates much more quickly, leading to mass transfer at a higher eccentricity and a significantly higher resulting mass transfer rate $\sim 10^{-3} M_\odot \text{ yr}^{-1}$. Such a model could be the progenitor of short-period quasi-periodic eruptions such as eRO-QPE2.

response to decreasing mass, respectively. For unstable mass transfer, the increase in radius drives a sharp increase in \dot{M}_\star , further increasing the stellar radius. This produces a runaway process which MESA is unable to solve numerically, leading to a very small timestep. The onset of unstable mass transfer is difficult to explicitly see in the radius evolution panels in Figures 5 & 6. However, a sharp rise in \dot{M}_\star is evident at the end stage of each stellar model, and is a signature of the onset of unstable mass transfer.

Figure 4 shows the convective velocity and specific entropy profiles for our two chosen heating models for one of our MESA calculations with the star on a mildly eccentric orbit ($e_i = 0.5$, $P_i = 7$ days). Three snapshots are shown: near ZAMS (t_i), at the onset of mass transfer (t_{RL}), and the final model near the onset of unstable mass transfer (t_f). All of our centrally heated models quickly become fully convective when the tidal heating rate becomes comparable to the stellar luminosity (Fig. 4). Once $\chi \approx 2$, mass transfer is immediately unstable: the star expands in response to mass loss, and MESA cannot continue to find solutions. On the contrary, when heating is evenly distributed per unit mass in most of the star, the star remains mostly radiative with a low-mass convective envelope on the exterior. Since the centrally heated models undergo unstable mass transfer once RLO commences, we focus our analysis on the more uniform heating models in

what follows.

3.1. Highly Eccentric Orbits

We adopt the same configuration as in our analytic model in §2 with a $M_\bullet = 7 \times 10^7 M_\odot$ point mass SMBH orbited by Sun-like ZAMS stars with an initial orbital period of 114.2 days. Figure 5 shows the stellar and orbital evolution for a range of initial tidal heating parameters $\chi_i = 2.6 - 3.4$, which also translates to a range of initial eccentricities ($e_i \sim 0.965 - 0.975$). For our MESA models, heating is gradually turned on for numerical stability, and reaches the full value in Equation 3 starting 100 years after t_{ZAMS} .

The left column in Figure 5 shows the stellar radius and orbital evolution before the onset of mass transfer, measured as a function of time since ZAMS. The right column shows the evolution of stellar mass, mass transfer rate, and stellar radius after RLO. For this range of χ_i , MESA can always find a stable mass transfer solution that lasts for $\sim 10^4$ yrs. Subsequently, the stellar evolution culminates when the radius increases as mass loss continues, driving a sharp increase in \dot{M}_\star , at which point MESA can no longer continue to model the dynamics of this runaway process.

Overall, we obtain stable mass transfer rates from MESA models similar to our analytics in Section 2, set by the tidal heating timescale instead of the gravitational wave timescale.

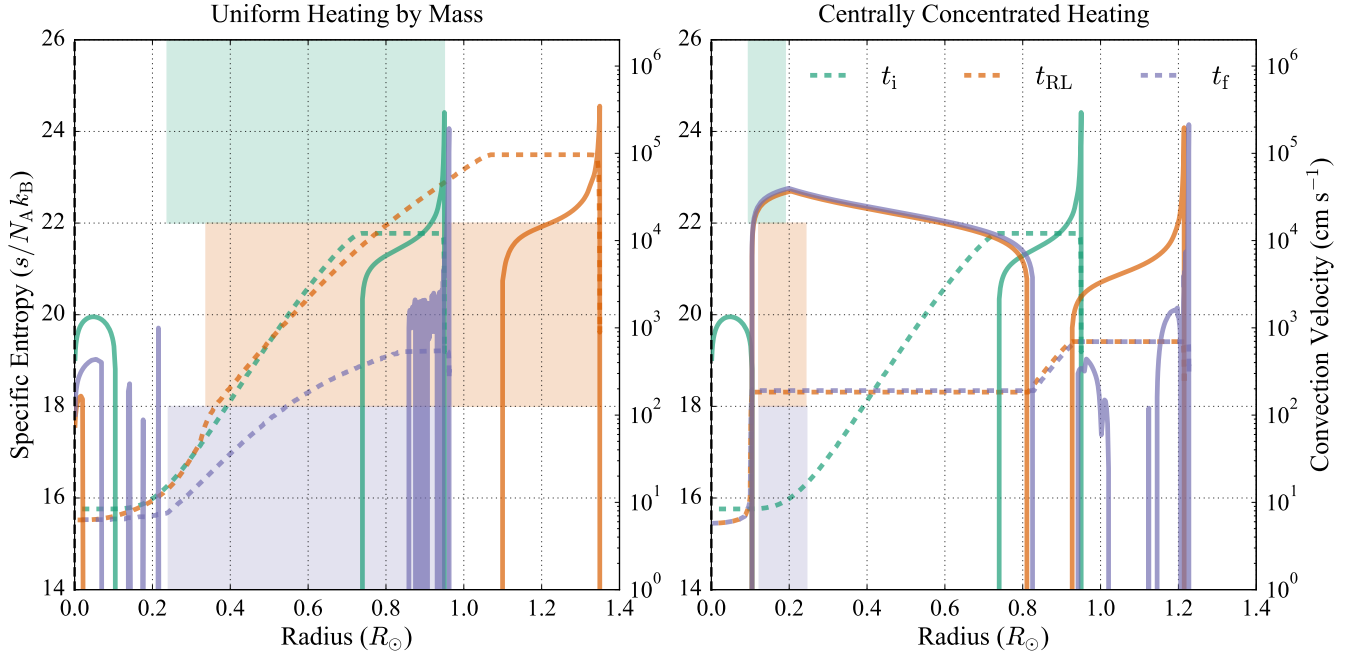


FIG. 4.— Internal stellar profiles of tidally heated stars (shown here: mildly eccentric, $e_i = 0.5$, $P_i = 7$ days, violet line in fig. 6) with the dashed lines showing specific entropy and solid lines showing convective velocity within the star. The *left* and *right* panels correspond to the (1) centrally concentrated and (2) uniformly throughout the star cases discussed in §3. The 3 different colors shown represent the stellar structure at different stages of stellar evolution: the green, orange, and purple profiles correspond to models closest to zero-age-main-sequence (t_i), beginning of Roche-lobe overflow (t_{RL}), and after unstable mass transfer sets in (t_f). The shaded regions represent the radial extent within which tidal heating energy is being deposited at each stage. Uniform heating throughout the star inhibits convection and allows for a phase of stable mass transfer, whereas centrally concentrated heating generates large convective regions, leading to unstable mass transfer.

Compared to our analytic model, which assumes stable mass transfer at all times, the star in our MESA model loses $\sim 20\%$ – 70% of its mass before the mass transfer becomes unstable (in the case of uniform heating per unit mass throughout most of the star). Models with higher χ_i tend to have higher \dot{M}_\star , and are more prone to unstable mass transfer for our phenomenological tidal heating model.

3.2. Mildly Eccentric Orbits

For stars on mildly eccentric orbits, as in §2, we adopt a $M_\bullet = 3 \times 10^6 M_\odot$ point mass SMBH orbited by Sun-like ZAMS stars with a range of eccentricities and orbital periods. Figure 6 shows stellar and orbital evolution with the same initial orbital parameters as in Figure 2: initial eccentricity 0.3 or 0.5 and orbital period of 4 or 7 days. Likewise, the *left* column in Figures 6 show the stellar radius and orbital evolution before the onset of mass transfer, measured as a function of time since ZAMS, and the *right* column shows the evolution of stellar mass, mass transfer rate, and stellar radius after RLO.

Like what we found in our analytic model (§2), the mass transfer rate here is set by the tidal heating timescale $\dot{M}_\star \sim 10^{-6} - 10^{-4} M_\odot/\text{yr}$, which results in a $\sim 10^5$ -year phase of stable mass transfer during which a Sun-like star can lose 40–60% of its mass before unstable mass transfer sets in. The behavior of \dot{M}_\star evolution in the MESA runs is also similar to our analytic calculations, where \dot{M}_\star always evolves secularly higher, until the mass transfer eventually becomes unstable, driving a sharp increase in \dot{M} .

4. DISCUSSION & SUMMARY

Stars in galactic nuclei can experience significant tidal heating due to their proximity to the central SMBH. For stars whose orbits reach sufficiently small pericenter distances relative to the tidal radius, the heating eventually causes runaway expansion of the star, and the star is destined to transfer mass to the SMBH. Motivated by the interplay of these physical processes, we developed an analytic model that describes the stable mass transfer solution in the presence of tidal heating, in which a star’s intrinsic response to mass loss is to shrink sufficiently in radius (unstable mass transfer is also possible, as we discuss below). The specific tidal heating models we use are based on solar mass stars, but many qualitative features of our evolutionary models are more broadly applicable. We then incorporated orbital changes due to gravitational waves and tides into a semi-analytic model of coupled stellar and orbital evolution. In parallel, we performed the same calculations using more realistic stellar models in MESA, with models for tidal heating included in the MESA calculations. The MESA models explicitly address whether mass transfer is stable or unstable since the internal stellar structure determines whether the star expands or contracts in response to mass loss. Our primary results, their implications, and avenues for future work are discussed below.

In standard models of stable mass transfer in binary systems, the mass transfer rate is set by the rate of angular momentum loss in the system, which drives the binary together (e.g., by gravitational wave emission or magnetic braking of stellar rotation). We have shown that for stars orbiting SMBHs there is a new stable mass transfer solution set by the tidal heating timescale $\tau_{\text{heat}} \sim E_\star / \dot{E}_{\text{tides}}$, in which $\dot{M}_\star \sim M_\star / \tau_{\text{heat}}$. We analytically derived the properties of this stable mass transfer

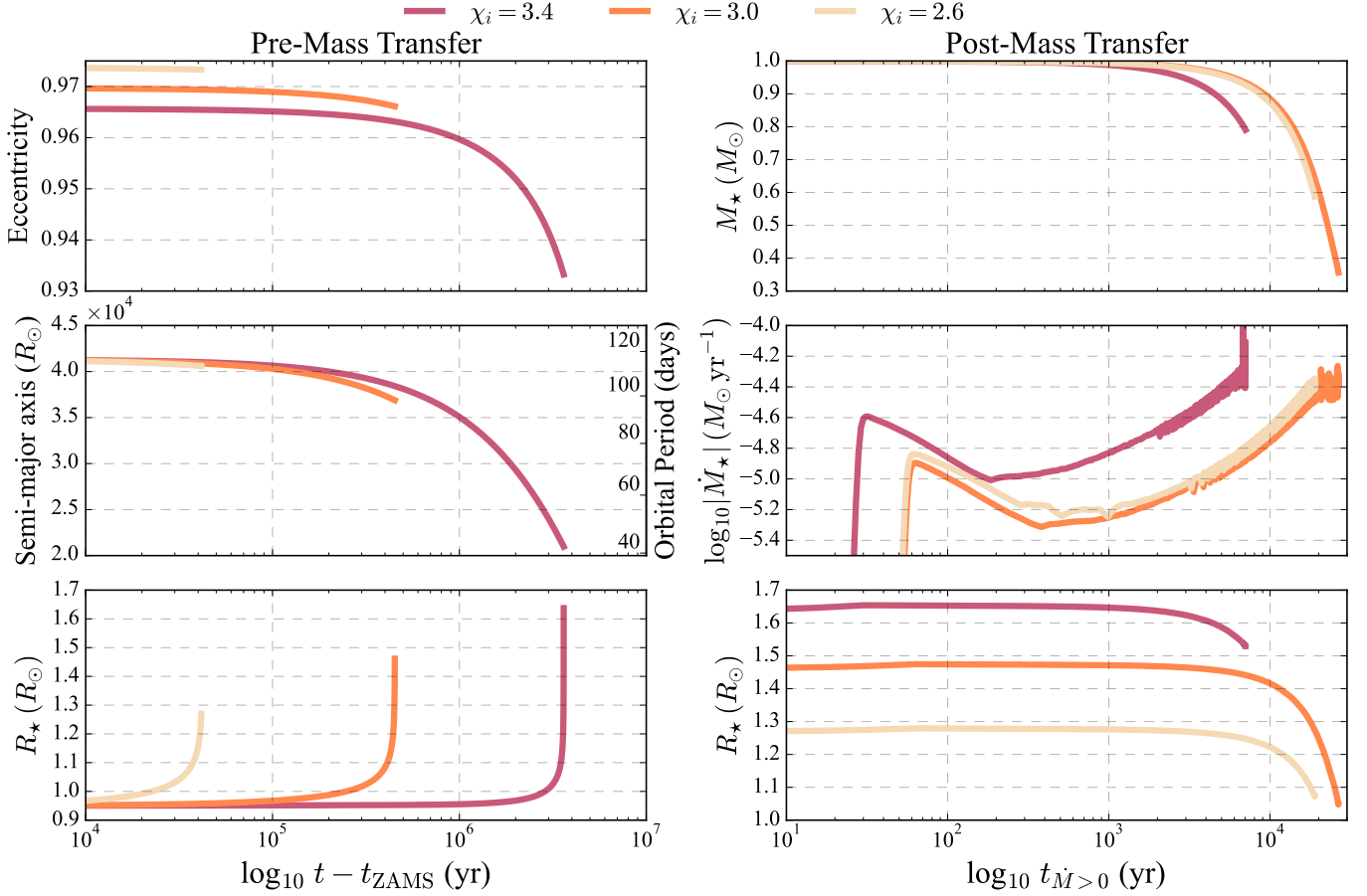


FIG. 5.— *Highly eccentric Orbits*: MESA solution for the evolution of orbital and stellar properties (eq. 11) before (left) and after (right) the onset of mass transfer at $r_p = a(1 - e) = 2r_t$. The models are subsets of those for which Figure 1 shows our simplified analytic model: a $1 M_\odot$ star at ZAMS orbiting a $7 \times 10^7 M_\odot$ SMBH, an initial orbital period $P_i = 114.2$ days, and a range of initial tidal heating parameters $\chi_i \equiv r_p/r_t$, which is equivalent to a range of initial eccentricities. We generally recover similar orbital and stellar evolution to models evolved analytically in Fig. 1. The MESA models end with the onset of unstable mass transfer, as indicated by the rapid rise in \dot{M}_\star in the right panel at the latest times.

solution (eqs. 7, 8 & 9; Fig. 1, 2 & 3) and verified it in MESA models (Fig. 5 & 6). Our results show that the tidal heating timescale is significantly less than the gravitational wave inspiral time unless the eccentricity at the onset of mass transfer is $\ll \sim 0.01$. Thus, stable mass transfer with tidal heating has a larger mass-transfer rate than mass transfer induced by gravitational wave orbital decay, significantly reducing the lifetime of the mass-transferring phase and increasing the luminosity of star-powered accretion in galactic nuclei.

For stars on highly eccentric orbits, our analytic model predicts that, if mass transfer is stable, it occurs for $10^3 - 10^5$ years with $\dot{M}_{\star, \text{para}}(t_{\text{MT}})/M_\star \sim 10^{-5} - 10^{-3} M_\odot/\text{yr}$; the mass transfer rate scales inversely with the orbital period at the onset of mass transfer and linearly with the tidal heating rate (eq. 7). Such systems would likely appear observationally as repeating nuclear transients in galactic nuclei, with emission powered by accretion of stellar debris lost at pericenter and/or circularization shocks associated with such debris. Our default models predict mass-transfer rates a factor of ~ 10 lower than needed to explain the luminosities of a system like ASASSN-14ko (Payne et al. 2021) which has been exhibiting persistent flares every ≈ 114 days over the past decade (ASASSN-14ko requires $\langle \dot{M} \rangle \sim 3 \times 10^{-3} M_\odot/\text{yr}^{-1}$ to power the flares by accretion). It is thus likely that many RNTs powered by tidally heated mass loss are fainter than the pTDE candidates de-

tected thus far. Different stellar models can, however, have significantly different tidal heating rates (e.g., Lee & Ostriker 1986 for polytropes), so a larger heating rate for some stellar models and/or evolutionary phases is plausible. The eccentric stable mass transfer model is essentially a gentler version of the partial-TDE picture, which has previously been used to explain the multi-wavelength flares of ASASSN-14ko (e.g. Payne et al. 2021; Cufari et al. 2022; Bandopadhyay et al. 2024). The two models differ in the following ways: tidal heating-induced RLO applies to stars whose pericenter distance approaches the tidal radius slowly as in the empty loss cone regime, or for stars that are dynamically placed on bound orbits with $2 \lesssim r_p/r_t \lesssim 5$. By contrast, if stars are scattered onto orbits with $1 \lesssim r_p/r_t \lesssim 2$, the calculations here are not applicable and instead the star undergoes a true partial tidal disruption. In the latter regime, the tidal heating generated mass loss is likely small compared to the matter directly stripped by the tidal forces (Bandopadhyay et al. 2025). Tidal heating-induced RLO is more difficult to simulate, but would be very useful to study directly with multi-dimensional simulations. The simulations to date that come the closest are those of Bandopadhyay et al. (2024); Liu et al. (2025) who studied repeated interactions between stars and a SMBH accounting for the tidally induced change to the stellar structure. The regime explored in this paper differs in that the initial stellar

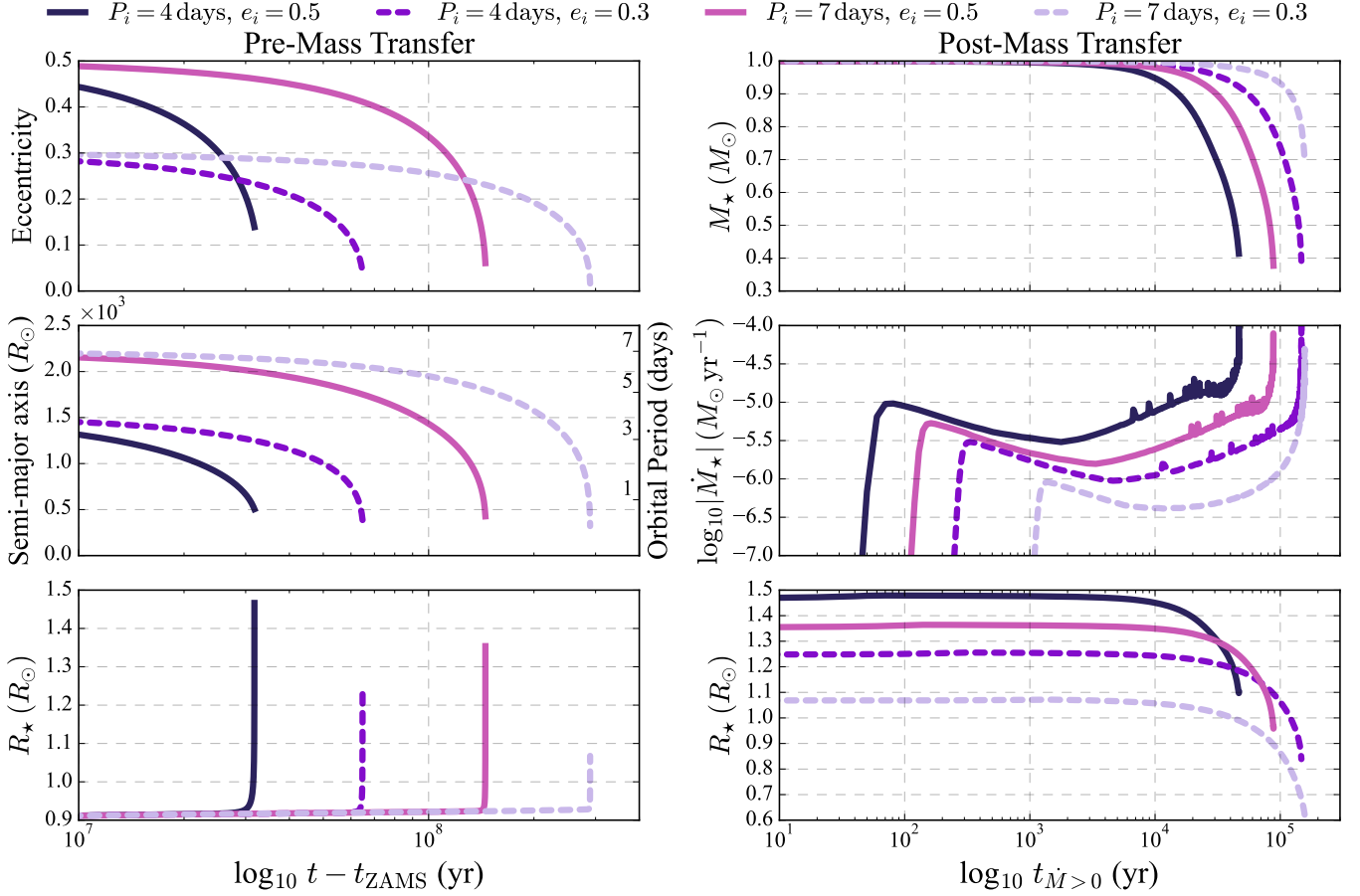


FIG. 6.— *Near-circular Orbits*: MESA solution for the evolution of orbital and stellar properties before (left) and after (right) the onset of mass transfer at $r_p = a(1 - e) = 2r_t$. The models shown are the same as for the analytic model in Figure 2: a $1M_\odot$ star at ZAMS orbiting a $3 \times 10^6 M_\odot$ SMBH, an initial eccentricity $e_i = 0.3$ (dashed lines) or $e_i = 0.5$ (solid lines) and an initial orbital period P_i of 4 or 7 days. We recover similar orbital and stellar evolution to models evolved analytically in fig. 2. The MESA models end with the onset of unstable mass transfer, as indicated by the rapid rise in \dot{M}_\star in the right panel at the latest times.

pericenter distance is larger, the star is tidally inflated prior to the onset of mass-transfer, the mass-loss per pericenter passage is generally lower, and the star will be roughly co-rotating with the orbit at pericenter by the onset of mass-transfer (though we do not explicitly model rotation).

For stars on near-circular orbits, our analytic model with a fiducial tidal heating prescription predicts that, if mass transfer is stable, it occurs for $\sim 10^4 - 10^6$ years with $\dot{M}_{\star, \text{circ}} \sim 10^{-6} - 10^{-4} M_\odot/\text{yr}$; the mass transfer rate scales with orbital eccentricity squared and linearly with the tidal heating rate (eq. 9). For sufficiently small eccentricity at the onset of mass transfer, the tidal heating timescale is longer than gravitational wave orbital decay, and thus the latter sets the stable mass transfer rate. Observationally, such stable mass transfer on a roughly circular orbit could power a persistent low-luminosity AGN. Indeed if the rate of producing stars on mildly eccentric orbits around SMBHs is $\sim 10^{-5} - 10^6 \text{ yr}^{-1}$ for a Milky Way mass galaxy (Linial & Sari 2023; Lu & Quataert 2023), a significant fraction of galaxies could host accretion powered by a mass-transferring star.

Interactions between the star and the disk it produced can also potentially power episodic flares once or twice per orbit (Lu & Quataert 2023). In particular, since the star's orbit is likely inclined to the equatorial plane of the SMBH spin, the disk formed by stellar mass transfer becomes aligned with the

SMBH spin by the Bardeen-Peterson effect (Bardeen & Petterson 1975). The star and its tidally stripped stellar debris will then collide with the disk it created on an inclined orbit, producing phenomenology similar to that found in recent work on QPEs (e.g. Linial & Metzger 2023; Tagawa & Haiman 2023; Yao et al. 2025). Our default tidal heating models predict stable mass transfer rates lower than what is necessary to explain the quiescent (between flare) emission in QPE sources such as GSN 069 and eRO-QPE2. As we have stressed throughout the paper, however, the tidal heating rate that sets the stable mass transfer rate in our models is uncertain. For example, inertial wave excitation can produce tidal heating rates that are several orders of magnitude larger than the internal gravity wave excitation implemented in this work (e.g. Barker 2020; Linial & Quataert 2024b). It is also plausible that nonlinear dissipation of the equilibrium tide energy (e.g., Weinberg et al. 2012) may become important at the large tidal energies that necessarily accompany RLO around SMBHs. If there are channels for stable mass transfer via tidal heating that produce $\dot{M}_{\star, \text{circ}} \sim 10^{-3} - 10^{-2} M_\odot/\text{yr}$ (which requires tidal heating rates ~ 100 times larger than our default model; see eq. 9 and Fig. 3), such a channel could account for the shortest period QPEs such as GSN 069 and eRO-QPE2 (Miniutti et al. 2019; Arcodia et al. 2021).³

³ Previous models of QPEs invoked unstable mass transfer to explain the

Recent discoveries of longer-period QPEs are associated with optically selected TDEs (Nicholl et al. 2024). By contrast, some of the shortest period QPEs, such as GSN 069 and eRO-QPE2, have quiescent (non-flaring) emission that is quite long-lived (Miniutti et al. 2023a,b) and it is less clear if these are standard tidal disruption events (TDEs; see, however, Guolo et al. 2025b who argue that GSN 069 is plausibly a TDE with an unusually long disk viscous time). The stable mass transfer model qualitatively explains this long-duration disk emission as well as the lack of other standard AGN features such as broad lines. It can also naturally explain the rapid onset of the quiescent emission because the accretion rate increases to the stable mass transfer value on the time it takes tidal heating to inflate the star a distance comparable to the scale-height of the stellar photosphere H , $\tau_{\text{MT}} \sim \tau_{\text{heat}}(H/R_\star)$, where τ_{heat} is the tidal heating timescale. If $\tau_{\text{heat}} \sim 100 - 1000$ years, as needed to explain the quiescent disk emission in QPEs, $\tau_{\text{MT}} \sim 0.1 - 1$ years is sufficiently short to explain the rapid onset of accretion in these systems. A quiescent disk fed by mass-loss from a star has an unusual optical-UV spectrum distinct from that of TDEs that may allow direct tests of this model (Lu & Quataert 2023) (for GSN 069, Guolo et al. 2025a favor a standard spreading accretion disk UV spectrum from $\approx 5 - 10$ eV but the difference between the star-fed disk and a spreading disk at those wavelengths is modest; see Fig. 4 of Lu & Quataert 2023; it is more pronounced at longer wavelengths). If RLO indeed powers some QPEs, it can only produce shorter period systems (\lesssim days). A prediction is that such shorter recurrence time systems would have systematically different quiescent disk emission than QPEs following optically selected TDEs, and should lack the early time optical emission seen in TDEs.

There is still large uncertainty as to where tidal heating energy is deposited inside a star for the large tidal amplitudes of interest in this work. Our MESA models are consistent with expectations that if tidal heating generates large convective regions, it will lead to unstable mass transfer. This is realized in our model by tidal heating concentrated in the center of a Sun-like star. By contrast, constant heating per unit mass throughout most of the star increases the size of the radiative zone (Fig. 4). This leads to an extended phase of stable mass transfer in MESA models. The true outcome of mass transfer in tidally heated stars will require more detailed calculations that properly evolve the tidal heating rate and its spatial distribution in the stellar interior as a function of time in response to the changing stellar structure. We defer this to future work.

The work presented here should be improved in a number of

ways. Indeed, we hope to have been forthright that our primary goal has been to assess the qualitatively new features that result from tidal heating in stars orbiting close to SMBHs. Many of the quantitative details of our predictions are uncertain and will require significantly more work. This includes the tidal heating rates themselves as well as the spatial distribution of the tidal heating in the stellar interior. In addition, our models of highly eccentric stable mass transfer are particularly idealized. Our MESA implementation approximates the tidal energy deposition as uniform throughout the entire orbital period, while in reality the tidal energy is deposited near pericenter and then thermalized by non-linear interactions. The mass loss itself will be impulsive as well, concentrated near pericenter. Whether such mass transfer is indeed stable for some stellar progenitors remains to be seen, but we suspect that our results about the stability of mass transfer for a given stellar structure are robust (the biggest uncertainty is then the structure of tidally heated stars). For example, the calculations of Bandopadhyay et al. (2025) of stellar response to impulsive mass stripping are consistent with the stability results in this paper: Bandopadhyay et al. (2025) find that lower mass stars, which have adiabatic indices comparable to structural polytropic indices, expand with mass loss while higher mass [radiative] stars contract. This is equivalent to our result that fully convective stars (with similar adiabatic and structural polytropic indices) undergo unstable mass transfer while radiative stars undergo stable mass transfer. Finally, our calculations neglect the interaction between the orbiting star and accretion disks formed in (unrelated) parabolic TDEs, many of which occur on the timescales of interest in this paper (Linial & Metzger 2023). It is unclear if the star approaching RLO can in fact survive its repeated collisions with TDE disks (Linial & Metzger 2023, 2024; Yao et al. 2025).

We thank Eric Coughlin, Jim Fuller, Itai Linial, Wenbin Lu, Brian Metzger, Selma de Mink, Aleksandra Olejak, and Enrico Ramirez-Ruiz for useful conversations, and Mathieu Renzo and Sunny Wong for helpful MESA suggestions. This work was supported in part by a Simons Investigator grant from the Simons Foundation (EQ). This research benefited from interactions at workshops funded by the Gordon and Betty Moore Foundation through grant GBMF5076 and through interactions at the Kavli Institute for Theoretical Physics, supported by NSF PHY-2309135.

REFERENCES

- Arcodia R., et al., 2021, *Nature*, **592**, 704
 Arcodia R., et al., 2022, *A&A*, **662**, A49
 Arcodia R., et al., 2024, *A&A*, **684**, A64
 Bandopadhyay A., Coughlin E. R., Nixon C. J., Pasham D. R., 2024, *ApJ*, **974**, 80
 Bandopadhyay A., Coughlin E. R., Nixon C. J., 2025, *arXiv e-prints*, p. [arXiv:2504.18614](#)
 Bardeen J. M., Petterson J. A., 1975, *ApJ*, **195**, L65
 Barker A. J., 2020, *MNRAS*, **498**, 2270
 Chakraborty J., Kara E., Masterson M., Giustini M., Miniutti G., Saxton R., 2021, *ApJ*, **921**, L40
 Chakraborty J., et al., 2024, *ApJ*, **965**, 12
 Chakraborty J., et al., 2025, *ApJ*, **983**, L39
 Cufari M., Coughlin E. R., Nixon C. J., 2022, *ApJ*, **929**, L20
 Cufari M., Nixon C. J., Coughlin E. R., 2023, *MNRAS*, **520**, L38
 Franchini A., et al., 2023, *A&A*, **675**, A100
 Ge H., Webbink R. F., Chen X., Han Z., 2015, *ApJ*, **812**, 40
 Gezari S., 2021, *ARA&A*, **59**, 21
 Goodman J., Dickson E. S., 1998, *ApJ*, **507**, 938
 Guolo M., Mummery A., Wevers T., Nicholl M., Gezari S., Ingram A., Pasham D. R., 2025a, *arXiv e-prints*, p. [arXiv:2501.03333](#)
 Guolo M., Mummery A., Ingram A., Nicholl M., Gezari S., Nathan E., 2025b, *arXiv e-prints*, p. [arXiv:2504.20148](#)
 Hameury J. M., King A. R., Lasota J. P., Auvergne M., 1994, *A&A*, **292**, 404
 Hills J. G., 1975, *Nature*, **254**, 295
 Hills J. G., 1988, *Nature*, **331**, 687
 Hinkle J. T., et al., 2024, *arXiv e-prints*, p. [arXiv:2412.15326](#)
 Hjellming M. S., Webbink R. F., 1987, *ApJ*, **318**, 794
 Krolik J. H., Linial I., 2022, *ApJ*, **941**, 24
 Kumar P., Goodman J., 1996, *ApJ*, **466**, 946
 Kumar P., Quataert E. J., 1998, *ApJ*, **493**, 412
 Lai D., 1997, *ApJ*, **490**, 847
 Lee H. M., Ostriker J. P., 1986, *ApJ*, **310**, 176
 Li G., Loeb A., 2013, *MNRAS*, **429**, 3040
 Linial I., Metzger B. D., 2023, *ApJ*, **957**, 34

high accretion rates needed in QPE models (Lu & Quataert 2023; Linial & Sari 2023). By showing that the stable mass transfer rate can be much larger in the presence of tidal heating, our results open up the space of progenitor models for QPEs to include stable mass transfer. This does not, of course, preclude that unstable mass transfer channels could still be viable as well.

- Linial I., Metzger B. D., 2024, *ApJ*, **973**, 101
 Linial I., Quataert E., 2024a, *MNRAS*, **527**, 4317
 Linial I., Quataert E., 2024b, *ApJ*, **974**, 67
 Linial I., Sari R., 2017, *MNRAS*, **469**, 2441
 Linial I., Sari R., 2023, *ApJ*, **945**, 86
 Liu Z., et al., 2023a, *A&A*, **669**, A75
 Liu C., Mockler B., Ramirez-Ruiz E., Yarza R., Law-Smith J. A. P., Naoz S., Melchor D., Rose S., 2023b, *ApJ*, **944**, 184
 Liu C., Yarza R., Ramirez-Ruiz E., 2025, *ApJ*, **979**, 40
 Lu W., Quataert E., 2023, *MNRAS*, **524**, 6247
 Lu W., Fuller J., Raveh Y., Perets H. B., Li T. S., Hosek Matthew W. J., Do T., 2021, *MNRAS*, **503**, 603
 MacLeod M., Ramirez-Ruiz E., Grady S., Guillochon J., 2013, *ApJ*, **777**, 133
 Mardling R. A., 1995a, *ApJ*, **450**, 722
 Mardling R. A., 1995b, *ApJ*, **450**, 732
 Miniutti G., et al., 2019, *Nature*, **573**, 381
 Miniutti G., Giustini M., Arcodia R., Saxton R. D., Read A. M., Bianchi S., Alexander K. D., 2023a, *A&A*, **670**, A93
 Miniutti G., Giustini M., Arcodia R., Saxton R. D., Chakraborty J., Read A. M., Kara E., 2023b, *A&A*, **674**, L1
 Nicholl M., et al., 2024, *Nature*, **634**, 804
 Paczyński B., 1971, *ARA&A*, **9**, 183
 Paxton B., Bildsten L., Dotter A., Herwig F., Lesaffre P., Timmes F., 2011, *ApJS*, **192**, 3
 Paxton B., et al., 2013, *ApJS*, **208**, 4
 Paxton B., et al., 2015, *ApJS*, **220**, 15
 Paxton B., et al., 2018, *ApJS*, **234**, 34
 Paxton B., et al., 2019, *ApJS*, **243**, 10
 Payne A. V., et al., 2021, *ApJ*, **910**, 125
 Payne A. V., et al., 2022, *ApJ*, **926**, 142
 Peters P. C., 1964, *Physical Review*, **136**, 1224
 Press W. H., Teukolsky S. A., 1977, *ApJ*, **213**, 183
 Rees M. J., 1988, *Nature*, **333**, 523
 Suková P., Zajaček M., Witzany V., Karas V., 2021, *ApJ*, **917**, 43
 Tagawa H., Haiman Z., 2023, *MNRAS*, **526**, 69
 Vick M., Lai D., 2018, *MNRAS*, **476**, 482
 Webb R., Young A. J., 2023, *MNRAS*, **518**, 3428
 Weinberg N. N., Arras P., Quataert E., Burkart J., 2012, *ApJ*, **751**, 136
 Wevers T., Pasham D. R., Jalan P., Rakshit S., Arcodia R., 2022, *A&A*, **659**, L2
 Wu Y., 2018, *AJ*, **155**, 118
 Xian J., Zhang F., Dou L., He J., Shu X., 2021, *ApJ*, **921**, L32
 Yao Y., et al., 2023, *ApJ*, **955**, L6
 Yao P. Z., Quataert E., Jiang Y.-F., Lu W., White C. J., 2025, *ApJ*, **978**, 91

This paper was built using the Open Journal of Astrophysics \LaTeX template. The OJA is a journal which provides fast and easy peer review for new papers in the `astro-ph` section of the

arXiv, making the reviewing process simpler for authors and referees alike. Learn more at <http://astro.theoj.org>.